OPEN

Quantitative Proteomic Analysis of Differentially Expressed Protein Profiles Involved in Pancreatic Ductal Adenocarcinoma

Kung-Kai Kuo, MD, PhD,† Chao-Jen Kuo, PhD,‡ Chiang-Yen Chiu,* Shih-Shin Liang, PhD,§|| Chun-Hao Huang,¶ Shu-Wen Chi,‡ Kun-Bow Tsai, MD,# Chiao-Yun Chen, MD,**†† Edward Hsi, PhD,‡‡ Kuang-Hung Cheng, PhD,§§ and Shyh-Horng Chiou, PhD‡||||¶¶*

Objectives: The aim of this study was to identify differentially expressed proteins among various stages of pancreatic ductal adenocarcinoma (PDAC) by shotgun proteomics using nano-liquid chromatography coupled tandem mass spectrometry and stable isotope dimethyl labeling.

Methods: Differentially expressed proteins were identified and compared based on the mass spectral differences of their isotope-labeled peptide fragments generated from protease digestion.

Results: Our quantitative proteomic analysis of the differentially expressed proteins with stable isotope (deuterium/hydrogen ratio, ≥2) identified a total of 353 proteins, with at least 5 protein biomarker proteins that were significantly differentially expressed between cancer and normal mice by at least a 2-fold alteration. These 5 protein biomarker candidates include α-enolase, α-catenin, 14-3-3 β, VDAC1, and calmodulin with high confidence levels. The expression levels were also found to be in agreement with those examined by Western blot and histochemical staining.

Conclusions: The systematic decrease or increase of these identified marker proteins may potentially reflect the morphological aberrations and diseased stages of pancreas carcinoma throughout progressive developments leading to PDAC. The results would form a firm foundation for future work concerning validation and clinical translation of some identified biomarkers into targeted diagnosis and therapy for various stages of PDAC.

Key Words: quantitative proteomics, pancreatic ductal adenocarcinoma, shotgun proteomics analysis, nano-liquid chromatography coupled tandem mass spectrometry, stable isotope dimethyl labeling

(*Pancreas* 2016;45: 71–83)

From the *Division of Hepatobiliary Surgery, Department of Surgery, Kaohsiung Medical University Hospital, †Center for Stem Cell Research, ‡Graduate Institute of Medicine, College of Medicine, §Department of Biotechnology, College of Life Science, and ||Center for Research Resources and Development, Kaohsiung Medical University, Kaohsiung, Taiwan; ¶Cell and Developmental Biology Program, Weill Graduate School of Medical Sciences, Cornell University, New York, NY; #Department of Pathology, Kaohsiung Municipal Hiao Kang Hospital; **Department of Radiology, Faculty of Medicine, College of Medicine, Kaohsiung Medical University; ††Department of Medical Imaging, Kaohsiung Medical University Hospital; ‡‡Department of Genome Medicine, College of Medicine, Kaohsiung Medical University; §§Institute of Biomedical Sciences, National Sun Yat-sen University, Kaohsiung; ||||Institute of Biological Chemistry, Academia Sinica, Taipei; and ¶¶Center for Infectious Disease and Cancer Research, Kaohsiung Medical University, Kaohsiung, Taiwan.

Received for publication November 11, 2014; accepted January 30, 2015.

Reprints: Shyh-Horng Chiou, PhD, Quantitative Proteomics Center and Graduate Institute of Medicine, Kaohsiung Medical University, No. 100, Shiquan 1st Rd, Sanmin Dist, Kaohsiung City 80708, Taiwan (e-mail: shchiou5tchiou@gmail.com); Kung-Kai Kuo, MD, PhD, Division of Hepatobiliary Surgery, Department of Surgery, Kaohsiung Medical University Hospital, Kaohsiung Medical University, No. 100, Shiquan 1st Rd, Sanmin Dist, Kaohsiung City 80708, Taiwan (e-mail: kuoksfo@yahoo.com.tw).

This study was funded by the National Science Council, Taipei, Taiwan and the Center for Stem Cell Research, Kaohsiung Medical University, Kaohsiung, Taiwan.

This study was supported by the National Science Council, Taipei, Taiwan (grant NSC101-2314-B-037-028-MY3 to S.H.C.). This study was also supported partially by Kaohsiung Medical University Aim for the Top Universities grant (grant number KMU-TP103E15, KMU-TP103G01, KMU-TP103G04, and KMU-TP103G05).

The authors declare no conflict of interest.

Supplemental digital contents are available for this article. Direct URL citations appear in the printed text and are provided in the HTML and PDF versions of this article on the journal's Web site (www.pancreasjournal.com).

Pancreatic ductal adenocarcinoma (PDAC), being ranked as the fourth leading cause of cancer mortality in the United States, remains one of the most devastating malignancies in patients with a 5-year survival rate of less than 5%.[1,2] Patients with this disease showed poor prognosis when diagnosed at an advanced stage due to the lack of reliable therapeutic targets and its high resistance to chemical as well as radiation therapy. Extended retroperitoneal dissection and/or intraoperative radiation have failed to improve their survival. The PDAC-related cancer death was reported to double in the past 2 decades. Numerous investigations underlying PDAC diagnosis as well as detection at an early stage based on protein markers carbohydrate antigen 19-9 and carcinoembryonic antigen in serum have been commonly reported in the literature. To date, these biomarkers are not specific for the detection of PDAC. Considerable literature on the molecular pathology revealed that various genetic alterations including the mutation of *SMAD4*, *p53*, K-*ras*, and telomere shortening detected in the pancreatic intraepithelial neoplasia (PanIN), the best characterized PDAC precursor lesion present in high percentage of cases, were associated with the progression of invasive PDAC.[3–7] Analysis of signaling components demonstrated that acinar cells, the major cellular component of the pancreas parenchyma, can be reprogrammed into PanIN or PDAC by the activated K-*ras* oncogene.[5,8–10]

It has been reported that gemcitabine, the commonly used chemotherapeutic agent for PDAC, exerts minor cytotoxic effects on tumor due to the triggering of escape route in signal transduction pathway.[11,12] The drug response and prolongation of survival are usually minimal (a few months or less). However, a recent study showed patients with pathologic cancer stage 1 (pTS1 ≤2 cm) could have 72% of the 5-year survival rate.[13] Therefore, general diagnosis or detection at an early stage of PDAC is considered to be imperative and crucial to improve clinical outcomes for PDAC patients. Furthermore, it is also critical and beneficial to discern practical and functional biomarkers coupled with the development of curative therapy for the effective management of PDAC.

Based on the current detection limit, the comprehensive global analysis of protein expression profiles by nano-liquid chromatography coupled tandem mass spectrometry (nano-LC-MS/MS) can be used to examine the potential biomarker candidates from total protein mixtures of various sample sources.[14,15] The determination of protein identity (protein ID) of interest lies in the tandem mass (MS/MS) spectra of peptide fragments, generated by digestion of proteins with cleavage-specific enzymes such as trypsin or some other well-characterized

proteases. Recently, the shotgun proteomics approach is capable of characterizing proteins directly from entire tissue or cell lysates.[16–18]

In this study, we have made an effort to characterize and compare the differentially expressed proteins between mouse mutant and normal wild-type strain during cancer progression to identify potential biomarker candidates by means of gel-free shotgun proteomic analysis coupled with stable isotope dimethyl labeling[14,18,19] and nano-LC-MS/MS.[19–21] Despite the fact that clinical sample analysis is the most optimal approach to provide more solid information for the application of translational medicine, numerous specimens from patients at different stages of PDAC are required to derive some statistical significance. Therefore, mouse models that recapitulate genetic backgrounds of human cancer are more expediently and justifiably used to conduct the survey of comparative proteomes owing to the advantage of genetic homogeneity and experimental reproducibility in mammalian mutant mice system. In addition, the comparative analysis at the immunohisto chemical (IHC) as well as messenger RNA (mRNA) level reported herein also facilitates further work to understand the underlying mechanism in tumor biology and subsequent validation and clinical translation of biomarkers with high prognostic values for targeted diagnosis and therapy in PDAC.

MATERIALS AND METHODS

Chemical Reagents and Antibodies

Trichloroacetic acid (TCA), trifluoroacetic acid (TFA), dithiothreitol, iodoacetamide, ethylenediaminetetraacetic acid, sodium deoxycholate, sodium fluoride, formaldehyde-H_2, formaldehyde-D_2, ammonium bicarbonate (NH_4HCO_3), and Triton X-100 were purchased from Sigma-Aldrich (St Louis, Mo). Acetonitrile (ACN) and sodium phosphate were obtained from Merck (Darmstadt, Germany). Formic acid (FA), sodium acetate, sodium cyanoborohydride, and sodium chloride (NaCl) were purchased from Riedelde Haven (Seelze, Germany). Protease inhibitors (Complete Mini) were purchased from Roche (Mannheim, Germany). Sodium dodecyl sulfate (SDS) and urea were purchased from Amresco (Solon, Ohio). Modified sequencing-grade trypsin for in-gel digestion was purchased from Promega (Madison, Wis). Quantitative reagent for protein contents was purchased from Bio-Rad (Hercules, Calif). Primary antibodies including anti–14-3-3 β (AB9730) and anti–α-catenin (AB19021) were purchased from Millipore (Bedford, Mass). TRIzol reagent and SuperScript III Reverse Transcriptase Kit were obtained from Invitrogen (Carlsbad, Calif). Smart Quant Green Master Mix Kit was purchase from Thermo (Waltham, Mass). Bicinchoninic acid protein assay kit (BCA kit) and primary anti–α-enolase antibody (PA5-21387) were purchased from Pierce biotechnology (Rockford, Ill). Immobilon Western Chemiluminescent HRP substrate kit, primary antibodies against glyceraldehyde 3-phosphate dehydrogenase (GAPDH) (MAB374) and PDGF receptor β (04-397), and secondary antibodies including peroxidase-conjugated antirabbit and antimouse IgG were purchased from Millipore (Bedford, Mass). Hematoxylin and eosin (H&E) were purchased from ScyTek Laboratories (Logan, Utah). Primary antibody against Muc1 (AJ1517a) was purchased from Abgent (San Diego, Calif). Primary antibody against HIF-1α (SC-10790) was purchased from Santa Cruz Biotechnology (Dallas, Tex). Biotinylated IgG (BA9500), Elite ABC reagent, and peroxidase substrate DAB kit were obtained from Vector Labs (Burlingame, Calif).

Establishment of *Pdx1-Cre*/*LSL*-K-*ras*^{G12D}/*p53*$^{L/L \text{ or } L/+}$ Experimental Mice Strain

All mice were housed in the appropriate plastic cages at 22° C ± 2°C with 55% humidity and 12-hour light/dark cycle in the Animal Care Facility at Kaohsiung Medicine University following the guidelines of the Institutional Animal Care and Use Committee. The animal use protocol has been reviewed and approved by the Institutional Animal Care and Use Committee. The conditional transgenic mice (*Pdx1-Cre*/*LSL*-K-*ras*^{G12D}/*p53*$^{L/L \text{ or } L/+}$) model was established as a platform to provide reliable pancreatic cancer tissue at various stages for protein analysis. Focal PDAC was recognized as early as the age of 2.5 weeks. To perform lineage tracing, the parental strains including B6.FVB-Tg(Ipf1-cre)1Tuv, FVB.129-Trp53^{tm1Brn}, and B6.129-K-*ras*^{tm4Tyj} mice (obtained from the National Cancer Institute [NCI] Mouse Models of Human Cancers Consortium [NCI-MMHCC] Repository) were used to generate a panel of compound mutant strains. First, the B6.FVB-Tg(Ipf1-cre)1Tuv mice were mated with FVB.129-Trp53^{tm1Brn} mice to generate recombined alleles of *Pdx1-Cre*/*p53loxp* mice. In another way, FVB.129-Trp53^{tm1Brn} mice were mated with B6.129-K-*ras*^{tm4Tyj}mice to generate recombined alleles of *LSL*-K-*ras*^{G12D}/*p53loxp* mice. Then, the *Pdx1-Cre*/*p53loxp* mice and *LSL*-K-*ras*^{G12D}/*p53loxp* mice were inbred to obtain *Pdx1-Cre*/*LSL*-K-*ras*^{G12D}/*p53*$^{L/L \text{ or } L/+}$ mice. For the purpose of tracing, Cre-recombinase expression was driven by the Pdx1 promoter. At the first step, we performed the record of survival time of *Pdx1-Cre*/*LSL*-K-*ras*^{G12D}/*p53*$^{L/L \text{ or } L/+}$ mice due to the natural death based on the tumor progression; furthermore, the normal mice used for the record of survival time were killed by CO_2 euthanasia at the end of a study. After that, we further collected the specimen of the *Pdx1-Cre*/*LSL*-K-*ras*^{G12D}/*p53*$^{L/L \text{ or } L/+}$ and normal mice killed by CO_2 euthanasia and subjected these specimen to the subsequent molecular analysis at the indicated time point (from week 2.5 through 3.5 and 5 to 10) based on tumor progression.

Mouse Genotyping and Recombined Allele Detection

Genotyping of *Pdx1-Cre*/*LSL*-K-*ras*^{G12D}/*p53*$^{L/L \text{ or } L/+}$ were performed by using oligonucleotide primers as described on Mouse Repository of National Cancer Institute at Frederick Web site (http://mouse.ncifcrf.gov/). Recombined alleles were detected by using genomic DNA extracted from mice tail as previously described.[22]

RNA Isolation, Complementary DNA Synthesis, and Quantitative Real-Time Polymerase Chain Reaction (PCR)

The expression level of mRNA was determined by real-time RT-PCR. Total RNA was extracted from fresh frozen mouse pancreas tissue using TRIzol reagent. Messenger RNA was reverse transcribed using SuperScript III Reverse Transcriptase Kit system and examined using Smart Quant Green Master Mix Kit in MJ Mini personal Thermal Cycler (Bio-Rad). The operation of PCR follows the conditions: initial hot start step of 2 minutes at 50°C and then 10 minutes at 95°C; denaturation at 95°C for 15 seconds, annealing at 60°C for 30 seconds and elongation at 72°C for 30 seconds for each cycle of 40 cycles; excessive reaction of 2 minutes at 50°C and then 10 minutes at 95°C for 2 cycles; melting curve of the final step read per 0.57°C from 55°C to 95°C. Primers used in this experiment were listed in Table 1.

Protein Extraction

Pancreas tissue specimens of mouse mutant or normal strain were homogenized with a Polytron homogenizer in 1.5 mL extraction buffer containing 10 mM Tris-HCl pH 7.4, 10 mM sodium phosphate, 150 mM NaCl, 0.1% SDS, 2 mM ethylenediaminetetraacetic acid, 1% sodium deoxycholate, 100 mM sodium fluoride,

TABLE 1. Sequences of Primer Used for Quantitative Real-Time PCR

Target Gene	Forward	Reverse
Eno1	CCTCTTTCCTTGCTTTGCAG	GACAGAGGGACTCTGCCTTG
Ctnna1	TCATGGCAGCAAAAAGACAA	AGTCCCGGTTGGCCTTATAG
Calm1	ACTGGGTCAGAACCCAACAG	CCTCGCGGATCTCTTCTTC
14-3-3 (Ywhab)	CCAGGCAGAAAGCAAAGTGT	GGGTGTGTAGGCTGCATTTC
VDAC1	TGGCTGGCTACCAGATGAAT	AATGGAGCCACCAAACTCTG
Cpa1	GACGAGGAGAAGCAGCAGAT	TACAAGCTGTGGGTGCTCTG
Ctrb1	ACTCCTGCCCAGTTCTCTGA	CCCAGGACTCCTTGCACTTA
Clps	TTCTGCTTGTGTCCCTCCTT	GTGTCATGTTGGCAGCATCT
Amylase 2a	TGCACAAGGTCTGGAAATGA	TCCACAGGTACTGCTTGTTCC
Pnliprp1	CTTTCTGACCCATCGACCAT	ATGCAGTTCACCTCCTCCAC
Cel	GGACAACACCTATGGGCAAG	GGCACCTCCATAGATCCAGA
GAPDH	AACTTTGGCATTGTGGAAGG	GGATGCAGGGATGATGTTCT

1% Triton X-100, and protease-inhibitor cocktail. The homogenates were transferred to 1.5-mL Eppendorf tubes and centrifuged at 13,000*g* for 20 minutes at 4°C to remove debris and insoluble material. Aliquots of the supernatants were assayed with bicinchoninic acid (BCA) protein assay kit to determine total protein concentration and then stored at −80°C until further analysis.

Dimethyl Labeling and Peptide Preparation

Volumes of lysates containing 100 μg of total proteins from tissues were adjusted to 60 μL and treated with 0.7 μL of 1 M dithiothreitol and 9.3 μL of 7.5% SDS at 95°C for 5 minutes before reduction. After the reaction, lysates were further treated with 8 μL of 50 mM iodoacetamide at room temperature for alkylation in the dark for 30 minutes; subsequently proteins were precipitated by adding 52 μL of 50% TCA and incubated on ice for 15 minutes. After removing the supernatant by centrifugation at 13,000*g* for 5 minutes, the collected proteins were washed with 150 μL of 10% TCA, vortexed and centrifuged at 13,000*g* for 10 minutes. The precipitated proteins were washed again with 250 μL distilled H_2O, vortexed, and centrifuged thrice under the same condition. The resultant pellets were resuspended with

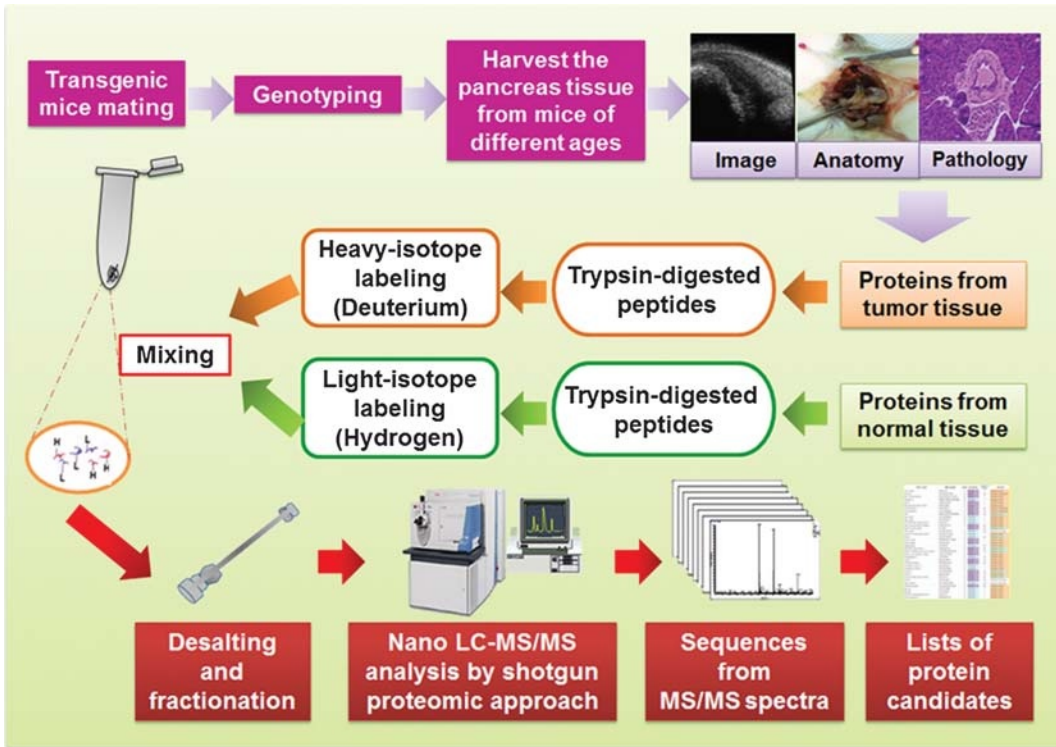

FIGURE 1. Experimental scheme of the procedures used for the confirmation of PDAC-bearing mice by histochemical, image and anatomical analyses, and screening of differentially expressed proteins at different progression stage of PDAC. After enzymatic digestion, peptides were differentially stable isotope dimethyl-labeled and combined before desalting and fractionation. The quantitative shotgun analysis of proteome changes from diseased and control groups was carried out by using HILIC-C18 peptide separation and nano-LC-MS/MS coupled with stable isotope dimethyl labeling.

50 mM NH_4HCO_3 (pH 8.5), then digested with 4 μg of trypsin for 8 hours at 37°C and further dried in a vacuum centrifuge to remove NH_4HCO_3. The lyophilized peptides from diseased and control groups redissolved in 180 μL of 100 mM sodium acetate at pH 5.5 were treated with 20 μL of 4% formaldehyde-H_2 and 20 μL 4% formaldehyde-D_2, respectively,[19–21] and mixed thoroughly. The mixtures were vortexed for 5 minutes, immediately followed by the addition of 10 μL of 0.6 M sodium cyanoborohydride and vortexed for 1 hour at room temperature. The resulting liquids acidified by 10% TFA/H_2O to pH 2.0 to 3.0 were applied onto the in-house reverse-phase C18 column pre-equilibrated with 200 μL of 0.1% TFA/H_2O (pH 2.0–3.0). The column was also washed with 200 μL of 0.1% TFA/H_2O (pH 3.0) and then eluted with a stepwise ACN gradient from 50% to 100% in 0.1% TFA at room temperature.

Hydrophilic Interaction Chromatography for Peptide Separation

Hydrophilic interaction chromatography (HILIC) was performed on an L-7100 pump system with quaternary gradient capability (Hitachi, Tokyo, Japan) using a TSK gel amide-80 HILIC column (2.0 × 150 mm, 3 μm; Tosoh Biosciences, Tokyo, Japan)[23–25] with a flow rate of 200 μL/min. Two buffers were used for gradient elution: solvent A, 0.1% TFA in water, and solvent B, 0.1% TFA in 100% ACN. The eluted fractions after being desalted from the in-house reverse-phase C18 column were each dissolved in 25 μL of solution containing 85% ACN and 0.1% TFA and then injected into the 20-μL sample loop. The gradient was processed as follows: 98% B for 5 minutes, 98% to 85% B for 5 minutes, 85% to 0% B for 40 minutes, 0% B for 5 minutes, 0% to 98 B for 2 minutes, and 98% B for 3 minutes. A total of 10 fractions were collected (1.2 mL for each fraction) and dried in a vacuum centrifuge.

Nano-LC-MS/MS Analysis

The lyophilized powders, reconstituted in 10 μL of 0.1% FA in H_2O, were analyzed by LTQ Orbitrap XL (Thermo Fisher Scientific, San Jose, Calif). Reverse-phase nano-liquid chromatography (nano-LC) separation was performed on an Agilent 1200 series nanoflow system (Agilent Technologies, Santa Clara, Calif). A total of 10-μL sample from collected fractions was loaded onto an Agilent Zorbax XDB C18 precolumn (0.35 mm, 5 μm), followed by separation using in-house C18 column (ID 75 μm × 15 cm, 3 μm). The mobile phases used were A 0.1% FA in water and B 0.1% FA in 100% ACN. The linear gradient from 5% to 95% of B over a 70-minute period at a flow rate of 300 nL/min was applied. The peptides were detected in the positive ion mode by applying a voltage of 1.8 kV to the injection needle. The MS was operated in a data-dependent mode, in which 1 full scan with m/z 400 to 1600 in the Orbitrap using a scan rate of 30 ms/scan. The fragmentation was performed using the collision-induced

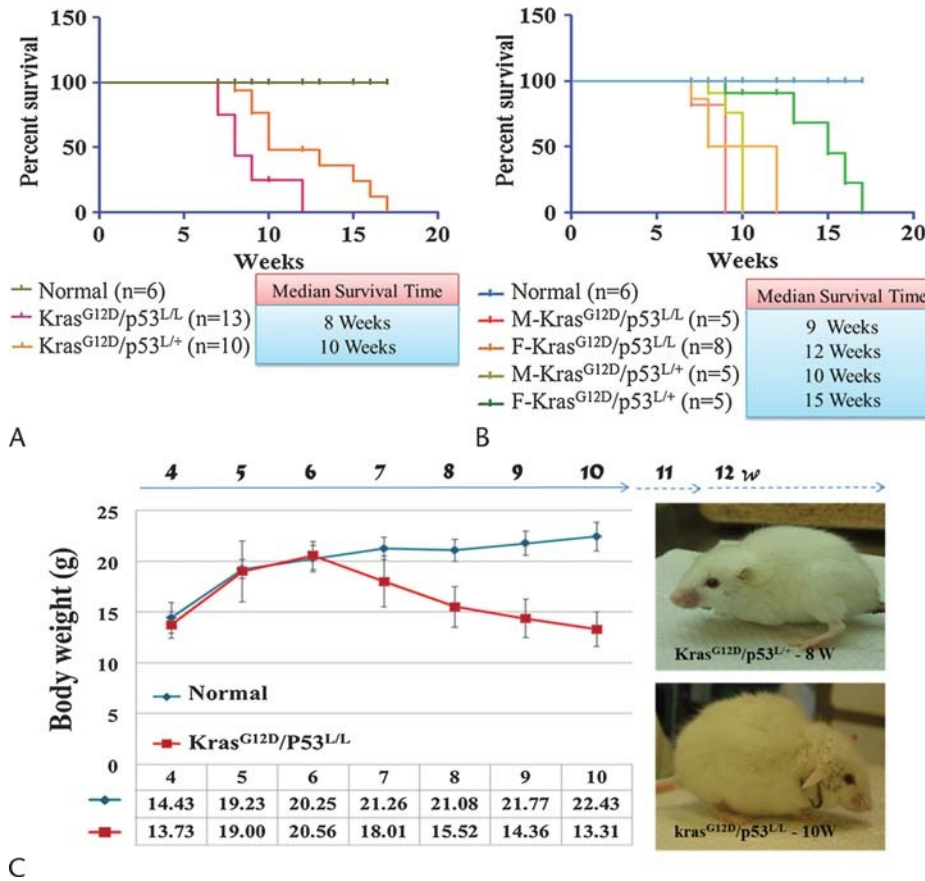

FIGURE 2. Mice succumbed to pancreatic tumor through K-*ras*^{G12D} activation and *p53* malfunction by genetic engineering technique. A, Kaplan-Meier overall survival analysis for normal mice and transgenic mice with K-*ras*^{G12D}/*p53*$^{L/L}$ or *p53*$^{L/+}$ genotypes. $P < 0.0001$. B, Kaplan-Meier overall survival analysis for male and female transgenic mice with K-*ras*^{G12D}/*p53*$^{L/L}$ as well as K-*ras*^{G12D}/*p53*$^{L/+}$ genotypes and normal mice. C, Two pictures on the right side showed the phenotype of tumor-bearing mice aged 8 or 10 weeks. The record of body weight in these 2 tumor-bearing mice was conducted for 10 consecutive weeks.

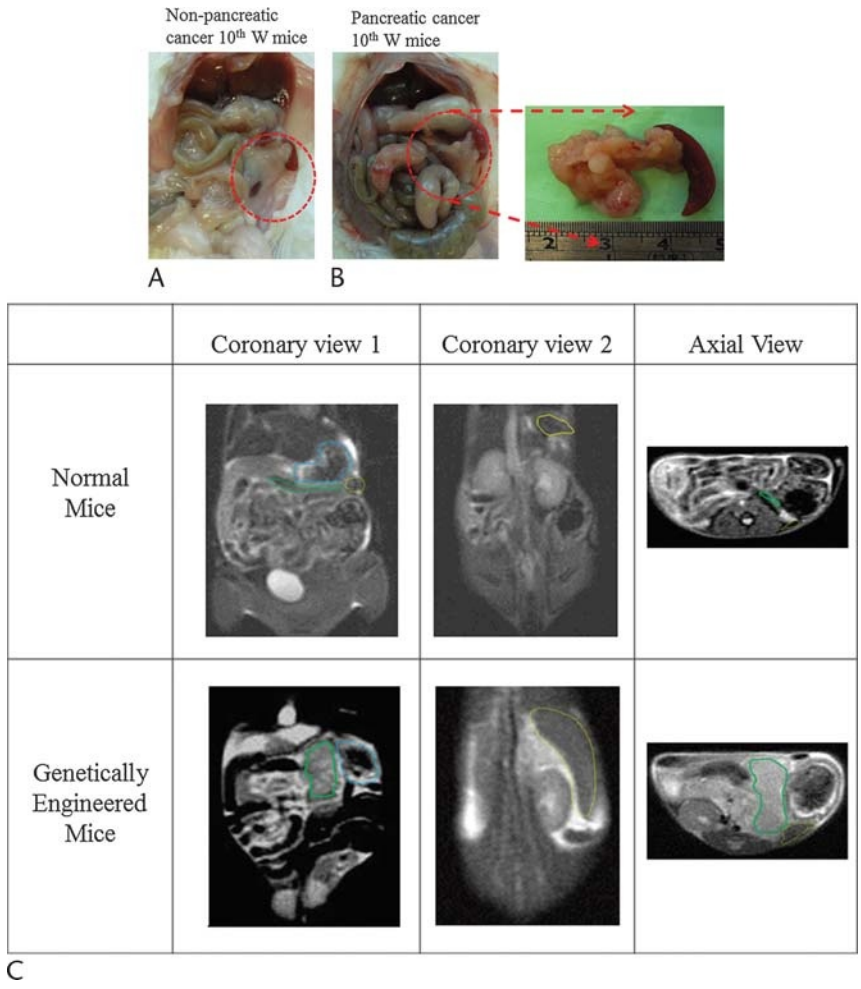

FIGURE 3. The formation of pancreatic tumor at week 10 was analyzed via dissection and 3.0-T MRI using a high-resolution animal coil (3.0 diameter). A, The circle with broken line illustrated the pancreas morphology of mice without the pancreatic tumor after dissection of the abdomen. B, The circle with broken line illustrated the pancreas morphology of tumor-bearing mice after dissection of the abdomen. C, The coronal view 1 and axial view of T2-weighted MRI scans showed a high-signal pancreas tumor (green circle with broken line) in the genetically engineered mice and the normal pancreas (green line) in the normal mice. The spleen and the stomach were also marked by the yellow and light blue dotted lines, respectively. In addition, splenomegaly showed in the genetically engineered mice.

dissociation mode with a collision energy of 35 V. A repeat duration of 30 seconds was applied to exclude the same m/z ions from being taken as the reselection for fragmentation. The Xcalibur software (version 2.0.7; Thermo Fisher Scientific, San Jose, Calif) was used for the management of instrument control, data acquisition, and data processing.

Protein Database Search and Characterization

Peptides were identified by peak lists converted from the nano-LC-MS/MS spectra by bioinformatics searching against mammal taxonomy in the Swiss-Prot databases for exact matches using the Mascot search program (http://www.matrixscience.com).[26,27] Parameters were set as follows: a mass tolerance of 10 ppm for precursor ions and 0.8 d for fragment ions, no missed cleavage site allowed for trypsin, carbamidomethyl cysteine as fixed modification, dimethylation specified as standard of the quantification, oxidized methionine, and deamidated asparagine/glutamine as optional modification. Peptides were considered positively identified if their Mascot individual ion score was higher than 20 ($P < 0.05$).

Subsequently, Mascot Distiller program (version 2.3; Matrix Science Ltd, London, United Kingdom) was applied to analyze the peptide quantification ratio (D/H) for control (hydrogen labeling) and diseased (deuterium labeling) groups by combining the peptide ratios matching the same sequence obtained from different fractions or at different retention time.[19]

Construction of Signaling Pathways and Network Analysis of Protein Interaction

The software program (www.ingenuity.com) from Ingenuity Pathways Analysis (IPA; Ingenuity Systems, Redwood City, Calif) was used for deriving the pathways and networks of protein interaction. Protein factors characterized by proteomic analysis were analyzed for their association with mapping related to canonical pathways deposited in the IPA library.

Western Blotting

An aliquot of 15 μg protein from each sample was separated on 10% or 12.5% polyacrylamide gels by 70 V for 12 minutes and

then 100 V for 2 hour and transferred to polyvinylidene difluoride membranes for 1.5 hour (Immobilon-P membrane; Millipore, Bedford, Mass). Membranes were blocked with 4% nonfat dry milk in Tris-buffered saline (TBS) 0.5% Tween 20 for 1 hour, and then incubated with the primary antibodies against α-enolase (1:500), 14-3-3 β (1:500), α-catenin (1:500), and GAPDH (1:1000) at 4°C overnight. The membranes were washed using TBS 0.5% Tween 20 and incubated with secondary antibodies conjugated with peroxidase against rabbit (1:2000) or mouse (1:2000) for 1 hour at room temperature. The signals on membrane were detected using Immobilon Western Chemiluminescent HRP (horseradish peroxidase) substrate kit for autoradiogram.

Hematoxylin and Eosin Stain, Immunohistochemistry, and In Vivo Imaging

Tissue samples were fixed in 4% buffered formalin for 12 hour, followed by washing with PBS, transferring to 70% ethanol, and then embedded in paraffin. Tissue sections were stained with hematoxylin and eosin (H&E). Immunohistochemical analysis

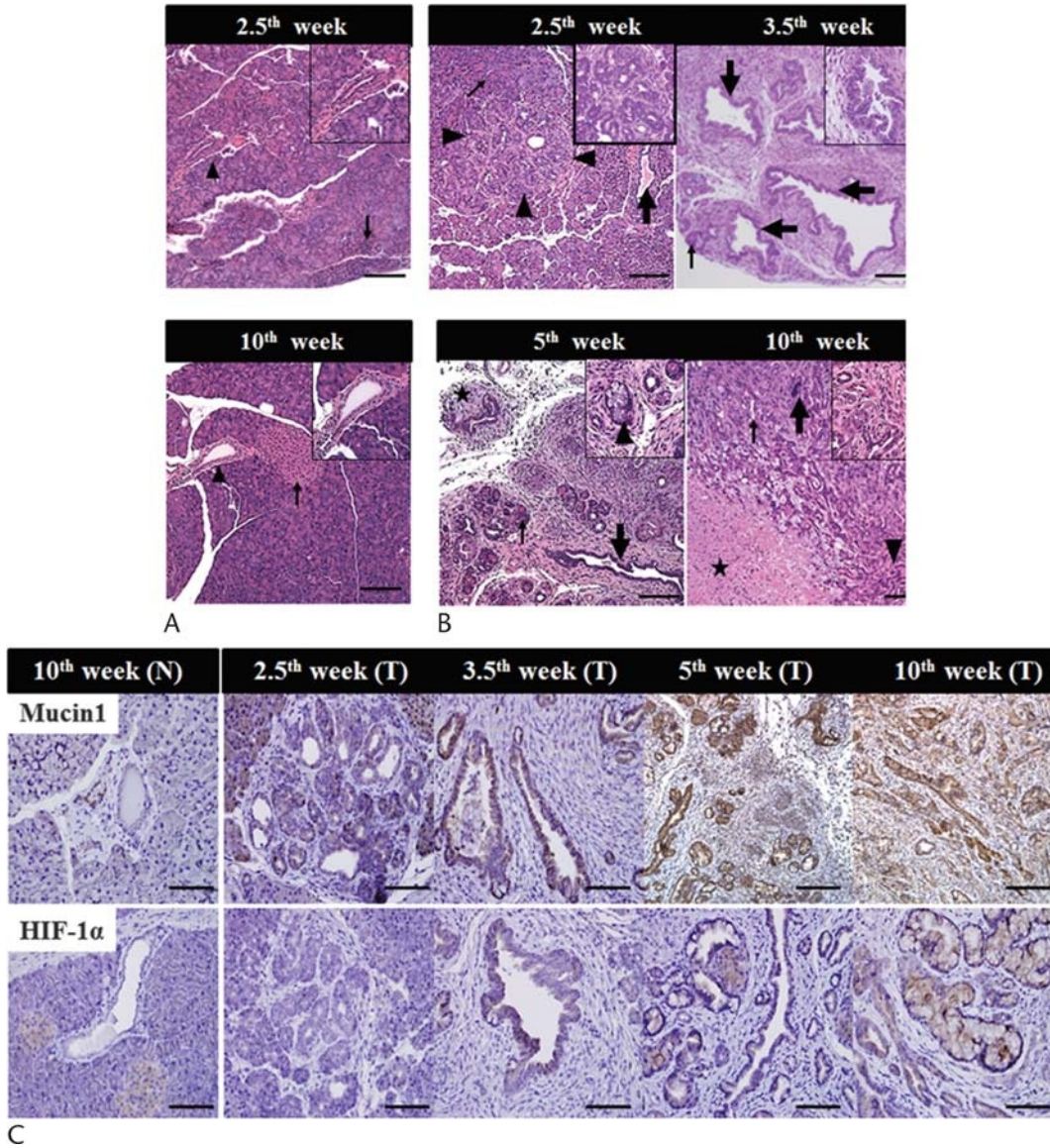

FIGURE 4. Histopathological features of pancreas tissue were examined by H&E staining in the normal (A) and tumor-bearing mice (B); tumor biomarkers (Mucin1 and HIF-1α) were characterized by IHC staining (C). A, Islets of Langerhans (thin arrows); the interlobular ducts (arrowheads). B, At week 2.5, malignant tumor foci could be identified in small portion of the whole pancreas (arrowhead). Furthermore, at week 3.5, the ducts dilated with multiple layers of tumor cells (thick arrows), which could grow in cribriform pattern as shown at the right upper panel. At week 5, the duct-like cancerous glands infiltrated the soft tissue and elicited a distinct desmoplastic stromal reaction (marked by star), and adenocarcinoma with mucoid cytoplasm was marked by an arrowhead and magnified at the upper right panel. At week 10, well-differentiated cancer cells in small tubules occupied most part of the entire glands as indicated by thin arrows and also enlarged at the right upper panel; some poorly differentiated cancer cells in cords could also be found as marked by a thick arrow. The scale bar represents 25 μm. C, The strong expression signals of Mucin1 and HIF-1α were observed on the morbid ductal cells at the late stage of PDAC. The scale bar is 50 μm.

TABLE 2. Characterization and Expression Levels (D/H Ratio) of Identified Proteins in the Progression of PDAC From Early to Late Stages in Different Sample Pairs Using Nano-LC-MS/MS Coupled With Stable Isotope Dimethyl Labeling

		D/H Ratio						
Protein ID	**Gene Symbol**	**(T1/T4)**	**(T2/T4)**	**(T3/T4)**	**(T1/N1)**	**(T2/N2)**	**(T3/N3)**	**(T4/N4)**
Calcium-binding proteins								
Calmodulin	Calm1	3.90	2.56	0.84	3.91	3.48	1.00	0.76
Protein S100-A6	S100A6	9.97	9.18		7.37	3.61		
Protein S100-A9	S100a9	4.97	5.86				7.16	
Protein S100-A11	S100a11	2.97	3.60		9.00	19.97	8.25	
Rho GTPase-regulated cytoskeletons								
Tubulin β-5 chain	Tubb5	2.10	2.61	0.94	5.25	2.53	2.08	1.07
Profilin-1	Pfn1	2.89	2.90	1.47	5.38	1.96	2.42	1.10
Myosin-9	Myh9	2.29	2.83	0.87	2.94	5.57	1.07	0.80
Cofilin-1	Cfl1	4.97	2.93	4.68	4.16	3.09	1.66	2.24
Development and progression of pancreatic cancer								
Vimentin	Vim	5.75	4.94	2.08	8.30	5.78	7.76	
Moesin	Msn	4.61	2.82	1.85	24.89	2.93		1.37
Peroxiredoxin-1	Prdx1	2.87	2.43	1.07	2.32	2.45	1.42	1.55
Galectin-1	Lgals1	3.33	3.19	0.76	6.39	1.66	2.14	
Epidermal growth factor signaling pathway								
14-3-3 protein β/α	Ywhab	3.58	2.09	0.67	4.64	2.41	1.42	0.83
14-3-3 protein ζ/δ	Ywhaz	3.53	1.96	1.30	4.41	2.41	1.26	1.38
14-3-3 protein gamma	Ywhag	3.23	1.96	0.82	4.06	2.00	1.39	1.26
14-3-3 protein θ	Ywhaq	2.87	2.01	0.86	4.08	1.79	1.25	1.67
14-3-3 protein ε	Ywhae	2.76	1.56	0.91	3.30	1.98	1.18	0.95
Glycolysis pathway								
Triose phosphate isomerase	Tpi1	3.05	2.04	1.30	4.18	1.43	1.35	1.04
L-lactate dehydrogenase A chain	Ldha	3.50	2.92	1.75	6.89	2.27	1.99	0.84
α-Enolase	Eno1	4.01	3.13	1.11	7.47	3.32	1.03	0.78
Phosphoglycerate kinase 1	Pgk1	4.71	2.17	0.94	2.23	1.12	1.60	1.25
Fructose-bisphosphate aldolase A	Aldoa	5.75	2.12	7.75	6.39	2.82		
Pyruvate kinase isozymes M1/M2	Pkm2	4.98	2.92	1.56	5.23	2.26	2.22	1.35
Pentose phosphate pathway								
Glucose-6-phosphate isomerase	Gpi	4.43	7.26	6.63	3.20	1.77	0.61	
Transketolase	Tkt	4.19	1.67	1.17	4.58	1.18	1.24	0.97
Tricarboxylic acid cycle								
Citrate synthase, mitochondrial	Cs	2.33	2.04	3.02	2.91	1.29	3.73	0.93
Succinate dehydrogenase (ubiquinone) flavoprotein subunit	Sdha	2.12	2.15	4.28	1.48	0.89		
Malate dehydrogenase, mitochondrial	Mdh2	2.52	1.14	1.58	2.47	0.76	1.19	0.75
Electron transport chain								
Cytochrome b5	Cyb5a	4.84		0.80	3.30	1.17		
Electron transfer flavoprotein subunit α	Etfa	3.09	1.18	1.39	0.85	0.59	0.75	1.01
Digestive enzymes								
Ribonuclease pancreatic	Rnase1	0.43	0.48	1.54	0.04	0.26	0.67	1.08
Carboxypeptidase A1	Cpa1	0.31	0.40	1.20	0.13	0.30	0.95	0.90
Pancreatic lipase-related protein 2	Pnliprp2	0.30	0.05	0.76	0.18	0.25	0.56	1.19
Chymotrypsinogen B	Ctrb1	0.29	0.72	1.16	0.12	0.50	1.53	1.37
Insulin-1	Ins1	0.29	0.27	1.73	1.31		3.54	
Bile salt-activated lipase	Cel	0.24	0.46	0.89	0.25	0.27	0.92	0.78
Glucagon	Gcg	0.22	0.46	1.24		7.41	3.19	
Colipase	Clps	0.21	0.31	0.60	0.08	0.21	1.71	0.99
Lithostathine-2	Reg2	0.35	2.80	2.43		0.60	0.68	0.85
Lithostathine-1	Reg1	0.15	0.56	1.34	0.29	0.63	1.64	0.93
Pancreatic lipase-related protein 1	Pnliprp1	0.15	0.33	0.80	0.24	0.56	1.12	0.70

(Continued on next page)

TABLE 2. *(Continued)*

Protein ID	Gene Symbol	D/H Ratio (T1/T4)	(T2/T4)	(T3/T4)	(T1/N1)	(T2/N2)	(T3/N3)	(T4/N4)
Pancreatic α-amylase	Amy2	0.12	0.31	0.94	0.09	0.16	0.65	1.03
Anionic trypsin-2	Prss2	0.09	0.73	1.85	0.07	0.37	1.64	1.12
Chymotrypsin-like elastase family member 2A	Cela2a	0.06	0.19	1.07	0.04	0.17	0.59	0.89
Cadherin-associated protein								
Catenin α-1	Ctnna1	3.29	1.05	0.56	3.99	3.05	1.08	1.58
Exchange of ions and molecules								
Voltage-dependent anion-selective channel protein 1	Vdac1	2.52	1.35	1.46	3.23	1.13	1.05	1.25

The indicated time points of groups 1 to 4 are 10, 5, 3.5, and 2.5 week.

D, deuterium labeling on peptide fragments of proteins from diseased groups; H, hydrogen labeling on peptide fragments of proteins from control of appropriate counterpart; T, tumor-bearing mice; N, normal control mice.

was conducted as previously described.[28] Magnetic resonance imaging (MRI) was performed using GE Signa VH/I scanner.

Statistical Analysis

Statistical analyses were performed using SPSS version 18.0 (SPSS, Chicago, Ill). The results were shown as mean (SD). The comparison between 2 groups was made using 1-way analysis of Students *t* test or paired *t* test. Log-rank (Mantel-Cox) test was used for the comparison of Kaplan-Meier plot for 2 conditions associated with mice survival. A *P* value of less than 0.05 was considered significant. Quantitative real-time PCR results were normalized to that of the housekeeping gene, glyceraldehyde-3-phosphate dehydrogenase.

Gene Expression Analysis

Gene expression analysis was carried out using the expression data set[29] in Oncomine database (www.oncomine.org) comparing PDAC to normal tissues.

RESULTS

In this study, we conducted a comparative proteome characterization of PDAC at the different stages by a bottom-up shotgun proteomic approach. A schematic representation of sample processing, separation, and the subsequent workflow concerning trypsin digestion, dimethyl labeling, and shotgun analysis is shown in Figure 1.

PDAC Progression of Transgenic Mice

To achieve the genetic requirements of K-ras^{G12D} expression in a tissue-specific manner for full malignant progression, we cross the engineered mice with *Pdx1-Cre/p53loxp and LSL*-K-ras^{G12D}/*p53loxp* to generate a conditional transgenic mice (*Pdx1-Cre*/*LSL*-K-ras^{G12D}/$p53^{L/L \text{ or } L/+}$) with a lox-stop-lox (LSL) cassette located between the promoter and the start codon of the K-ras^{G12D} open reading frame. Genotype-specific alterations of pancreatic tissues investigated by comparative molecular analysis indicated the presence of the correct Pdx1-Cre fragment and the low baseline of *p53* and mutated K-ras^{G12D}, as shown in the Supplementary Figure S1, http://links.lww.com/MPA/A391. After the growth of normal and transgenic mice at the age of 7 weeks, all K-ras^{G12D}/$p53^{L/+}$mice were susceptible to PDAC between ages 8 and 17 weeks (median survival time, 10 weeks), whereas K-ras^{G12D}/$p53^{L/L}$ mice with 8 weeks of median survival were more susceptible to PDAC, and their weight reduced markedly at week 8 (Fig. 2A, C). As far as sex difference is concerned, male K-ras^{G12D}/$p53^{L/+}$ mice with 10 weeks of median survival yielded to PDAC earlier than female K-ras^{G12D}/$p53^{L/+}$ mice with 15 weeks of median survival. In a similar manner, male K-ras^{G12D}/$p53^{L/L}$ mice showing 9 weeks of median survival also succumbed to PDAC earlier than female K-ras^{G12D}/$p53^{L/L}$ mice with 12 weeks of median survival time (Fig. 2B). Based on this result, we demonstrated that female mice outsurvived male mice when they succumbed to pancreas malignant tumor.

For the purpose of tracking the progression and status of PDAC, we further examined the histological changes of pancreas tissue between normal and transgenic mice at the different stages. The anatomical studies in Figures 3A and B revealed that transgenic mice at the week 10 bore larger solid tumors than normal mice in the pancreas tissue after dissection of the abdomen, as illustrated by the circle with a broken line. Noninvasive method using image analysis by MRI in Figure 3C also clearly displayed a larger dark tumor area, which indicated a bona fide tumor and highlighted by the green solid line on the transgenic mice when compared with the image shown on the normal mice. Detailed analysis by using H&E staining further demonstrated that interlobular ducts (arrowheads) are composed of a single layer of cuboid epithelial cells (being further magnified at the right upper panel); islets of Langerhans (thin arrows) and lobular structures of acinar cells are clearly observed in the normal mice from week 2.5 to 10, as shown in Figure 4A.

However, when transgenic mice are killed at week 2.5, malignant tumor foci could be identified in a small portion of the whole pancreas (arrowhead), as shown in Figure 4B. Furthermore, at week 3.5, the ducts dilated with multiple layers of tumor cells (thick arrows), which could grow in cribriform pattern as shown at the right upper panel. At week 5, the duct-like cancerous glands infiltrated the soft tissue and elicited a distinct desmoplastic stromal reaction (marked by an asterisk), and adenocarcinoma with mucoid cytoplasm was marked by an arrowhead and magnified at the upper right panel. At week 10, well-differentiated cancer cells in small tubules occupied most part of the entire glands as indicated by thin arrows and also enlarged at the right upper panel; some poorly differentiated cancer cells in cords could also be found, as marked by a thick arrow. Figure 4C showed that the strong expression of cancer progression-related signals, Mucin1 and HIF-1α,[30,31] were observed on the morbid ductal cells at the late stage of PDAC from week 5 to 10. Immunofluorescence analysis also extended to the primary cells purified from pancreatic tumor of 10 weeks mice and displayed Mucin1-positive signal (Supplementary Figure S2, http://links.lww.com/MPA/A391).

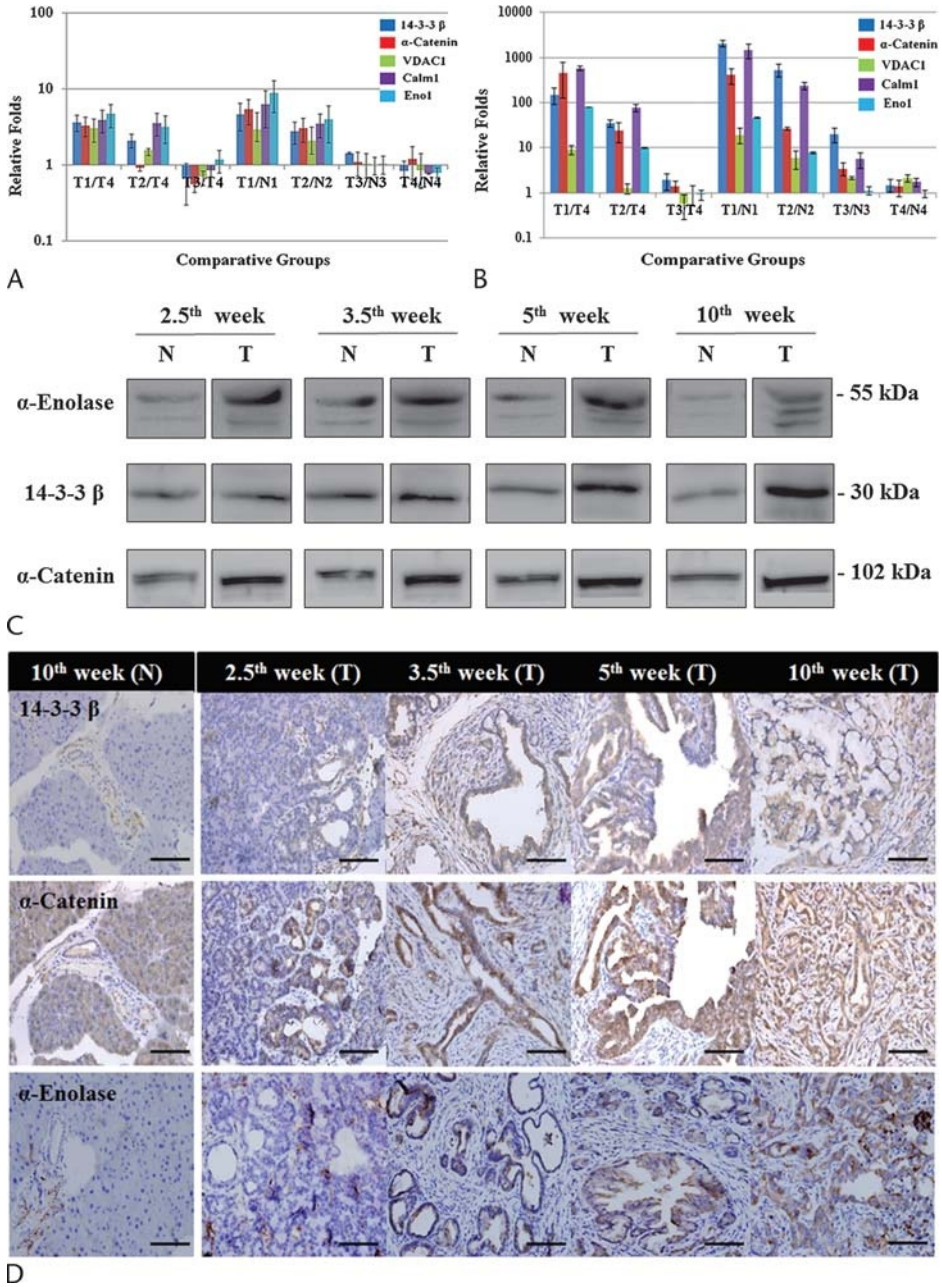

FIGURE 5. The differentially expressed proteins with upregulated patterns at the indicated time points in the normal and tumor-bearing mice were identified by comparative proteome analysis using nano-LC-MS/MS that corresponds to the results analyzed by quantitative real-time PCR and Western blot. All values were normalized to the appropriate control groups, which were set to 1.0. T indicates tumor-bearing mice; N, normal control mice; the indicated time points of the 1 to 4 groups are 10, 5, 3.5, and 2.5 weeks. A, The 5 representative upregulated proteins were dramatically accompanied with PDAC progression in tumor-bearing mice. B, The 5 representative mRNA expression levels examined by quantitative real-time PCR increased concomitantly with PDAC progression. C, The 3 representative upregulated proteins were confirmed and examined by Western blot. D, The 3 representative upregulated proteins were confirmed and examined by IHC staining.

Identification of Differentially Expressed Proteins by Comparative Proteomics Analysis

Based on these solid results of PDAC formation in our established mouse model, we conducted comparative proteome analysis to elucidate whether 1 or more factors play important roles in the progression of PDAC. Initially, 100 μg of total proteins isolated form pancreatic tissues of normal or tumor-bearing mice at different progression stages of PDAC was collected for trypsin digestion and dimethyl labeling. Respective tryptic peptide samples were mixed in a 1:1 (w/w) ratio and loaded to the reverse-phase C18 column for desalting and enrichment. To reduce the complexity of peptide population and facilitate the characterization performed by a single LC-MS/MS run, the enriched peptides were subject to HILIC separation based on polarity difference, and then harvested into 10 fractions. Peptides identified by the Mascot search program (http://www.matrixscience.com)[26,27] were accepted if their individual ion score was higher than 20,

which had been a cutoff point used for the lower-quality MS/MS spectra.[32–34]

When the differentially expressed proteins with confident identification based on peptide mass fingerprinting were completed, the peptide quantification ratio (D/H) was obtained using Mascot Distiller program[19,20,35] by merging data from each elution profile into 1 file that combined the same sequence matched by more than 1 peptide harvested from different fractions or at different retention time and charge state. Herein, characterization and expression levels (D/H ratio) of identified proteins in the progression of PDAC from early to late stages in different sample pairs using nano-LC-MS/MS coupled with stable isotope dimethyl labeling were shown in Table 2. The comparative global proteome analysis was listed in the Supplementary Table, http://links.lww.com/MPA/A392. Based on the quantitative results of dimethyl labeling using deuterium and hydrogen on tryptic peptides, a total of 59 upregulated (D/H ratio, ≥2) and 32 downregulated (D/H ratio, ≤0.5) proteins were identified in tumor-bearing mice at week 5 when compared with the expression level at the same indicated time point in the normal mice, as shown in T2/N2 group. With the advent of advanced stage of tumor, a total of 87 upregulated (D/H ratio, ≥2) and 31 downregulated (D/H ratio, ≤0.5) proteins were identified in tumor-bearing mice at week 10 when compared with the expression level at the same indicated time point in the normal mice, as shown in T1/N1 group.

In addition, the differential expression level of proteins accompanied with the progression of PDAC was further evaluated from week 2.5 to 10 in tumor-bearing mice. A total of 120 upregulated (D/H ratio, ≥2) and 40 downregulated (D/H ratio, ≤0.5) were identified in tumor-bearing mice at week 10 when compared with the expression level at week 2.5, as shown in T1/T4 group. Furthermore, a total of 69 upregulated (D/H ratio, ≥2) and 20 downregulated (D/H ratio, ≤0.5) were identified in tumor-bearing mice at week 5 when compared with the expression level at week 2.5, as shown in T2/T4 group. Figure 5A demonstrated that 5 representative proteins including 14-3-3 β, α-enolase, α-catenin, VDAC, and calmodulin were dramatically upregulated in T1/T4, T2/T4, T1/N1, and T2/N2 groups. These results were in agreement with mRNA expression level by quantitative real-time PCR analysis (Fig. 5B) and validated by Western blot and IHC staining (Fig. 5C, D).

Construction of Signaling Pathways and Network Analysis of Protein Interaction

The shotgun proteomics approach reported herein demonstrated a prospective potential application to monitor the expression level of a large number of cellular proteins and offer some novel candidate proteins complementary to previously identified target proteins in the literature. Using a combined panel of these identified proteins enables us to further cluster them into possible networks based on the biochemical characterization for examining some disease-oriented factors involved in the signaling connection governing the development and progression of the PDAC. In Figure 6, these identified proteins mapped to canonical pathways from the IPA (Ingenuity Systems) library were shown in red color to indicate the upregulation and green color to indicate the downregulation, and also displayed with different shapes to indicate the different functions. All the gray arrows indicate the biological interrelationships between these molecules. All arrows in Figure 6 were supported by at least 1 reference from the literature, textbooks, or canonical information stored in the Ingenuity Knowledge Base.

As illustrated in the possible association of molecular network, Ywhaz (14-3-3 protein ζ/δ) simultaneously interacted with Lgals1 (galectin-1), Eno1 (α-enolase), TUBA1A (tubulin α-1A chain), Vim (vimentin), S100A6 (protein S100-A6), ANXA1 (annexin A1), and EIF3F (eukaryotic translation initiation factor 3 subunit F). Therefore, PDAC was not characterized with a singular enzymatic or cytoskeleton alteration but with a series of complex and diverse functional upregulation or downregulation.

Expression of the Identified Biomarker Candidates in Human PDAC

To further investigate the potential of these identified candidates for clinical application, we analyzed the expression data set[29] comparing human PDAC to normal pancreas tissues. Among the top candidates, α-enolase and 14-3-3 protein β are significantly upregulated in PDAC tumors (n = 39), indicating that our results can be validated in patient samples (Fig. 7).

DISCUSSION

The transgenic mice we generated were successfully induced to promote PDAC progression and initiation by the forced activation of oncogene K-*ras*^{G12D} and deletion of tumor suppressor gene *p53*$^{L/L}$. It was based on the previous human genetic studies that 95% and 50% of human PDAC carried K-*ras* and *p53* mutation. As shown in Figure 4, the earlier event of PDAC was revealed as small foci of cancerous glands followed by well-differentiated adenocarcinoma with obvious desmoplastic reaction and the development of poorly differentiated PDAC. Various grades of metaplasia or PanINs could also be identified just near the main cancerous tissue, which is very similar to that of human PDAC progression.[36] In addition, an alternative approach by IHC staining was also used to examine the presence of Mucin1 and HIF-1α, as their aberrant

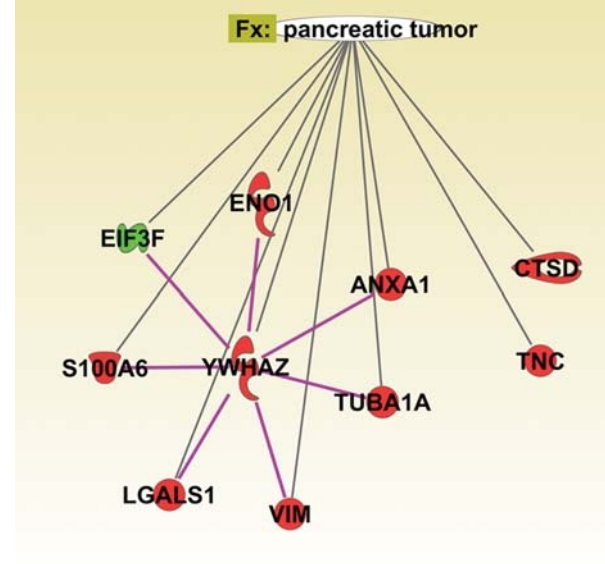

FIGURE 6. Schematic representation of derived pathways associated with pancreatic cancer. These identified proteins mapping to the canonical pathways from IPA (Ingenuity Systems) library were used for building the possible connection network. Identified proteins with upregulation and downregulation are displayed in red and green, respectively, and have different shapes to indicate different functions. The biological interrelationships between molecules were represented as arrows. All drawn arrows were cited and supported by at least 1 reference from the literature, textbooks, or canonical information stored in the Ingenuity Knowledge Base.

expression has been suggested to be involved in the progression,[30] invasion, and metastasis of pancreatic cancer.[31]

When the PDAC model was established and confirmed, we subjected the pancreatic cancerous tissue to identify potential biomarker candidates by comparing the differentially expressed proteins among various stages of tumor-bearing and normal mice during cancer progression. It has been well-documented that this approach can detect differentially expressed proteins at relatively low abundance.[37–40] In the Supplementary Table, http://links.lww.com/MPA/A392, our results demonstrated that oncogenic signaling of the K-$ras^{G12D}/p53^{L/L}$ forced expression led to the remarkable changes of translational level at the indicated time points.

Of these expressed molecular signatures in T1/T4 group, α-enolase, a well-defined tumor-related, and glycolytic enzyme, was found. α-Enolase has been considered to be a PDAC-associated antigen[41] and a potential diagnostic marker of pancreatic cancer.[42,43] Recently, this enzyme has been shown to be the promising target for new immunotherapeutic strategies in the cure of malignant tumor.[44] Furthermore, energy utilization-related enzymes such as glycolysis pathway (pyruvate kinase isozymes M1/M2, L-lactate dehydrogenase, fructose-bisphosphate aldolase A, phosphoglycerate kinase 1, α-enolase, triose phosphate isomerase), tri-carboxylic acid cycle (malate dehydrogenase, citrate synthase, succinate dehydrogenase), electron transport chain (cytochrome b5, flavoprotein subunit α), calcium-binding proteins (protein S100A6, A9, A11), and Rho GTPase-regulated cytoskeletons (myosin-9, cofilin-1, tubulin β5, profiling-1) were upregulated, as shown in Table 2.

Correspondingly, the function of K-ras^{G12D} on the regulation of glucose metabolism for energy supply in pancreatic cancer was also documented.[41] A significant proportion of functional proteins identified by comparative global survey in our high-throughput analysis including moesin, vimentin, epidermal growth factor signaling pathway (14-3-3 ε, 14-3-3 σ, 14-3-3 ζ/δ, 14-3-3 θ), galectin-1, and peroxiredoxin-1 were found to be associated with the development and progression of pancreatic cancer reported previously.[41,45–51] On the other hand, digestive enzymes such as carboxypeptidase A1, pancreatic lipase-related protein 2, chymotrypsinogen B, insulin-1, bile salt-activated lipase, colipase, pancreatic lipase-related protein 1, and pancreatic α-amylase were found to be downregulated, as shown in Table 2. The mRNA level examined by quantitative real-time PCR also corroborated this result as shown in the Supplementary Figure S3, http://links.lww.com/MPA/A391. The dramatic downregulation of pancreas-secreted enzymes may possibly result from the fact that acinar cells, the major cellular component of the pancreas parenchyma, were converted to ductal-like cancerous glands and lost the physiological function at the late stage of pancreatic cancer (Fig. 4B).

In terms of the functional classification of these identified proteins, several novel proteins including 14-3-3 β, α-catenin, voltage-dependent anion-selective channel protein 1 (VDAC1), calmodulin, and α-enolase in T1/T4 group, which were not reported previously to be involved in PDAC formation, were identified in our studies and also increasingly upregulated in T2/T4, T1/N1, and T2/N2 groups, as shown in Table 2. These 5 factors at the transcriptional and translational level were also concomitant

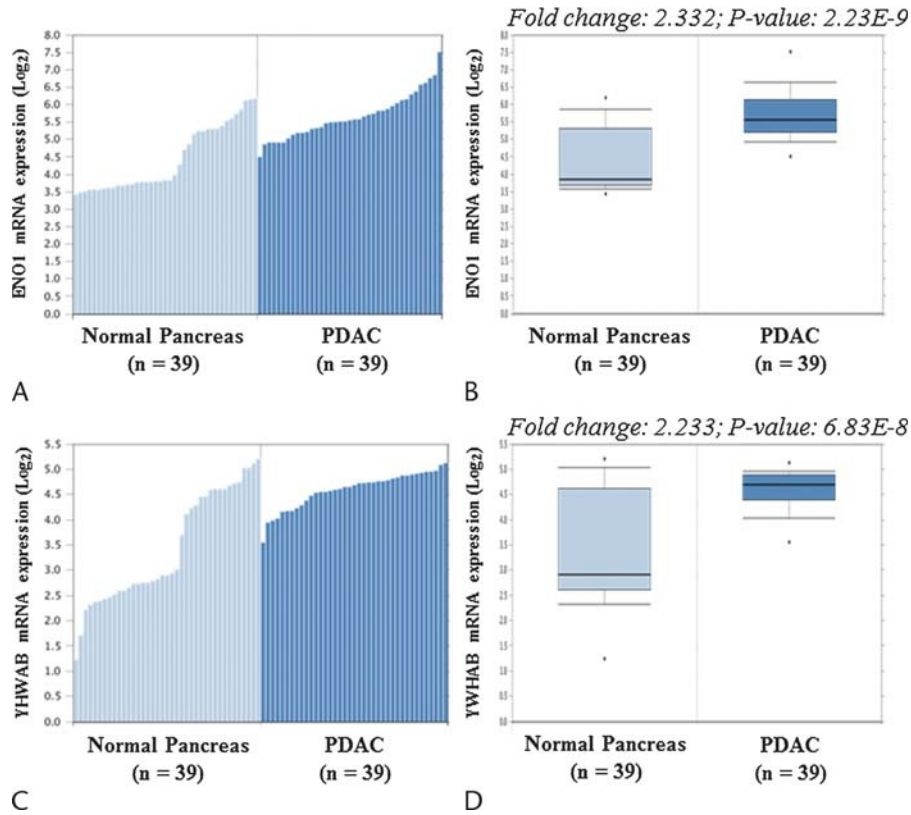

FIGURE 7. Expression of the identified biomarker candidates in human PDAC. A and B, mRNA expressions of α-enolase (Eno1) is significantly higher in PDAC tumors (n = 39) than in normal pancreas tissues (n = 39). C and D, mRNA expressions of 14-3-3 β (Ywhab) is significantly higher in PDAC tumors (n = 39) than in normal pancreas tissues (n = 39). The Oncomine database (www.oncomine.org) was used to analyze gene expression in the expression data set[29] comparing PDAC to normal tissues.

with PDAC progression, as validated in Figure 5. Furthermore, the analysis of human data in Figure 7 suggested that some of the potential biomarkers we identified using quantitative proteomic analysis and the PDAC mouse model, such as α-enolase and 14-3-3 β, may play important roles in PDAC tumorigenesis and could be useful for clinical application in the future. Connection network of identified proteins analyzed by IPA further demonstrated that α-enolase and 14-3-3 protein ζ/δ was involved in the pancreatic tumor. Although several novel proteins identified by our shotgun approach were not linked to the canonical network, the importance of these unmapped proteins remained to be elucidated and the potential of these proteins serving as candidate biomarkers will be validated by subjecting them to verification and validation using ion scanning of peptides measured and quantified in multiple reaction monitoring mode of nano-LC-MS/MS.

Chen et al have reported[52] that by analyzing pancreatic fluid obtained from the endoscopic retrograde cholangiopancreatography, PDAC patients with elevated levels of S100A8 or A9 in the ductal fluid, a near absence of pancreatic enzymes, and high levels of mucins were found to have significantly worse prognosis.[52] Our data also showed compatible results. Mice at late stage had much higher levels of S100A8, A9, and low detectable amylase. Other studies have used resected human PDAC tissue to identify putative biomarkers; however, the sizes of most resected tumors were larger than 2 cm (≥T2).[53–55] When tumor size increases, it usually associates with either lymph nodes or distal organs metastases. Therefore, proteins from these studies probably represented biomarkers for diseases progression. One merit of our study is to have designed an intermediate stage (aged 5 weeks). Our putative 5 proteins (α-enolase, 14-3-3 β, VDAC1, calmodulin, and α-catenin) from proteomics study were shown to be overexpressed constitutively in tissue on the approach of both quantitative PCR and Western blots as disease progressed. Recently, some studies have also shown that sera or pancreatic tissues from various transgenic mice model could be used for the discovery of novel protein biomarkers.[56,57] However, it is difficult to compare those results with ours because the altered genetic constructions were different in these models. Our transgenic mice model could develop cancerous foci within the shortest period when compared with others.[56,57] Theoretically, it is plausible to assume that the fast-growing tumor in this model might have a benefit that these overexpressed proteins in the connection networks should have direct or powerful influences on pancreatic tumorigenesis.

Collectively, the comparative proteome data from the mouse model harboring K-*ras*^{G12D} mutation and loss of *p53* may not only provide a novel approach to further elucidate the disease-oriented factors underlying the development of PDAC and the associated metabolic signaling pathways, but also identify potential and valuable biomarker candidates useful for future diagnosis, prognosis, and new potential alternatives for mechanism-based targets therapy.

ACKNOWLEDGMENT

The authors thank the core facility grant from the quantitative proteomics center (National Science Council grant 99-2745-B-037-005 to S.H.C.) at the Center for Research Resources and Development, Kaohsiung Medical University, under the auspices of the National Science Council.

REFERENCES

1. Jemal A, Siegel R, Xu J, et al. Cancer statistics, 2010. *CA Cancer J Clin*. 2010;60:277–300.
2. Li D, Xie K, Wolff R, et al. Pancreatic cancer. *Lancet*. 2004;363: 1049–1057.
3. DiGiuseppe JA, Hruban RH, Offerhaus GJ, et al. Detection of K-*ras* mutations in mucinous pancreatic duct hyperplasia from a patient with a family history of pancreatic carcinoma. *Am J Pathol*. 1994;144:889–895.
4. Gidekel Friedlander SY, Chu GC, Snyder EL, et al. Context-dependent transformation of adult pancreatic cells by oncogenic K-*ras*. *Cancer Cell*. 2009;16:379–389.
5. Hruban RH, Wilentz RE, Kern SE. Genetic progression in the pancreatic ducts. *Am J Pathol*. 2000;156:1821–1825.
6. van Heek NT, Meeker AK, Kern SE, et al. Telomere shortening is nearly universal in pancreatic intraepithelial neoplasia. *Am J Pathol*. 2002;161: 1541–1547.
7. Maitra A, Fukushima N, Takaori K, et al. Precursors to invasive pancreatic cancer. *Adv Anat Pathol*. 2005;12:81–91.
8. Zhu L, Shi G, Schmidt CM, et al. Acinar cells contribute to the molecular heterogeneity of pancreatic intraepithelial neoplasia. *Am J Pathol*. 2007; 171:263–273.
9. De La O JP, Emerson LL, Goodman JL, et al. Notch and Kras reprogram pancreatic acinar cells to ductal intraepithelial neoplasia. *Proc Natl Acad Sci U S A*. 2008;105:18907–18912.
10. Habbe N, Shi G, Meguid RA, et al. Spontaneous induction of murine pancreatic intraepithelial neoplasia (mPanIN) by acinar cell targeting of oncogenic Kras in adult mice. *Proc Natl Acad Sci U S A*. 2008;105: 18913–18918.
11. Kern SE, Shi C, Hruban RH. The complexity of pancreatic ductal cancers and multidimensional strategies for therapeutic targeting. *J Pathol*. 2011; 223:295–306.
12. Adesso L, Calabretta S, Barbagallo F, et al. Gemcitabine triggers a pro-survival response in pancreatic cancer cells through activation of the MNK2/EIF4E pathway. *Oncogene*. 2013;32:2848–2857.
13. Egawa S, Toma H, Ohigashi H, et al. Japan pancreatic cancer registry; 30th year anniversary: Japan pancreas society. *Pancreas*. 2012;41: 985–992.
14. Chiou SH, Wu CY. Clinical proteomics: current status, challenges, and future perspectives. *Kaohsiung J Med Sci*. 2011;27:1–14.
15. Ideker T, Thorsson V, Ranish JA, et al. Integrated genomic and proteomic analyses of a systematically perturbed metabolic network. *Science*. 2001;292:929–934.
16. Washburn MP, Wolters D, Yates JR 3rd. Large-scale analysis of the yeast proteome by multidimensional protein identification technology. *Nat Biotechnol*. 2001;19:242–247.
17. McCormack AL, Schieltz DM, Goode B, et al. Direct analysis and identification of proteins in mixtures by LC/MS/MS and database searching at the low-femtomole level. *Anal Chem*. 1997;69:767–776.
18. MacCoss MJ, McDonald WH, Saraf A, et al. Shotgun identification of protein modifications from protein complexes and lens tissue. *Proc Natl Acad Sci U S A*. 2002;99:7900–7905.
19. Wu CJ, Chen YW, Tai JH, et al. Quantitative phosphoproteomics studies using stable isotope dimethyl labeling coupled with IMAC-HILIC-NANOLC-MS/MS for estrogen-induced transcriptional regulation. *J Proteome Res*. 2011;10:1088–1097.
20. Santos HM, Kouvonen P, Capelo JL, et al. Isotopic labelling of peptides in tissues enhances mass spectrometric profiling. *Rapid Commun Mass Spectrom*. 2012;26:254–262.
21. Boersema PJ, Aye TT, van Veen TA, et al. Triplex protein quantification based on stable isotope labeling by peptide dimethylation applied to cell and tissue lysates. *Proteomics*. 2008;8:4624–4632.
22. Jackson EL, Willis N, Mercer K, et al. Analysis of lung tumor initiation and progression using conditional expression of oncogenic K-*ras*. *Genes Dev*. 2001;15:3243–3248.

23. Yoshida T. Peptide separation in normal phase liquid chromatography. *Anal Chem*. 1997;69:3038–3043.
24. Yoshida T. Calculation of peptide retention coefficients in normal-phase liquid chromatography. *J Chromatogr A*. 1998;808:105–112.
25. Alpert AJ. Hydrophilic-interaction chromatography for the separation of peptides, nucleic acids and other polar compounds. *J Chromatogr*. 1990;499:177–196.
26. Perkins DN, Pappin DJ, Creasy DM, et al. Probability-based protein identification by searching sequence databases using mass spectrometry data. *Electrophoresis*. 1999;20:3551–3567.
27. Hirosawa M, Hoshida M, Ishikawa M, et al. MASCOT: multiple alignment system for protein sequences based on three-way dynamic programming. *Comput Appl Biosci*. 1993;9:161–167.
28. Bardeesy N, Cheng KH, Berger JH, et al. Smad4 is dispensable for normal pancreas development yet critical in progression and tumor biology of pancreas cancer. *Genes Dev*. 2006;20:3130–3146.
29. Badea L, Herlea V, Dima SO, et al. Combined gene expression analysis of whole-tissue and microdissected pancreatic ductal adenocarcinoma identifies genes specifically overexpressed in tumor epithelia. *Hepatogastroenterology*. 2008;55:2016–2027.
30. Rachagani S, Torres MP, Kumar S, et al. Mucin (Muc) expression during pancreatic cancer progression in spontaneous mouse model: potential implications for diagnosis and therapy. *J Hematol Oncol*. 2012;5:68.
31. Zhao X, Gao S, Ren H, et al. Hypoxia-inducible factor-1 promotes pancreatic ductal adenocarcinoma invasion and metastasis by activating transcription of the actin-bundling protein fascin. *Cancer Res*. 2014; 74:2455–2464.
32. Thingholm TE, Jensen ON, Robinson PJ, et al. SIMAC (sequential elution from IMAC), a phosphoproteomics strategy for the rapid separation of monophosphorylated from multiply phosphorylated peptides. *Mol Cell Proteomics*. 2008;7:661–671.
33. Hou W, Ethier M, Smith JC, et al. Multiplexed proteomic reactor for the processing of proteomic samples. *Anal Chem*. 2007;79:39–44.
34. Pichler P, Kocher T, Holzmann J, et al. Peptide labeling with isobaric tags yields higher identification rates using iTRAQ 4-plex compared to TMT 6-plex and iTRAQ 8-plex on LTQ Orbitrap. *Anal Chem*. 2010;82: 6549–6558.
35. Webster J, Oxley D. Protein identification by maldi-tof mass spectrometry. *Methods Mol Biol*. 2012;800:227–240.
36. Shi G, DiRenzo D, Qu C, et al. Maintenance of acinar cell organization is critical to preventing Kras-induced acinar-ductal metaplasia. *Oncogene*. 2013;32:1950–1958.
37. Unwin RD, Craven RA, Harnden P, et al. Proteomic changes in renal cancer and co-ordinate demonstration of both the glycolytic and mitochondrial aspects of the Warburg effect. *Proteomics*. 2003;3: 1620–1632.
38. Craven RA, Stanley AJ, Hanrahan S, et al. Proteomic analysis of primary cell lines identifies protein changes present in renal cell carcinoma. *Proteomics*. 2006;6:2853–2864.
39. Wu CJ, Hsu JL, Huang SY, et al. Mapping n-terminus phosphorylation sites and quantitation by stable isotope dimethyl labeling. *J Am Soc Mass Spectrom*. 2010;21:460–471.
40. Huang SY, Tsai ML, Wu CJ, et al. Quantitation of protein phosphorylation in pregnant rat uteri using stable isotope dimethyl labeling coupled with IMAC. *Proteomics*. 2006;6:1722–1734.
41. Ying H, Kimmelman AC, Lyssiotis CA, et al. Oncogenic Kras maintains pancreatic tumors through regulation of anabolic glucose metabolism. *Cell*. 2012;149:656–670.
42. Zhou W, Capello M, Fredolini C, et al. Mass spectrometry analysis of the post-translational modifications of alpha-enolase from pancreatic ductal adenocarcinoma cells. *J Proteome Res*. 2010;9:2929–2936.
43. Cappello P, Tomaino B, Chiarle R, et al. An integrated humoral and cellular response is elicited in pancreatic cancer by alpha-enolase, a novel pancreatic ductal adenocarcinoma-associated antigen. *Int J Cancer*. 2009; 125:639–648.
44. Capello M, Ferri-Borgogno S, Cappello P, et al. α-Enolase: a promising therapeutic and diagnostic tumor target. *FEBS J*. 2011;278:1064–1074.
45. Cui Y, Wu J, Zong M, et al. Proteomic profiling in pancreatic cancer with and without lymph node metastasis. *Int J Cancer*. 2009;124:1614–1621.
46. Cao D, Maitra A, Saavedra JA, et al. Expression of novel markers of pancreatic ductal adenocarcinoma in pancreatic nonductal neoplasms: additional evidence of different genetic pathways. *Mod Pathol*. 2005;18: 752–761.
47. Kawahara T, Hotta N, Ozawa Y, et al. Quantitative proteomic profiling identifies dpysl3 as pancreatic ductal adenocarcinoma-associated molecule that regulates cell adhesion and migration by stabilization of focal adhesion complex. *PLoS One*. 2013;8:e79654.
48. Yamazaki K, Takamura M, Masugi Y, et al. Adenylate cyclase-associated protein 1 overexpressed in pancreatic cancers is involved in cancer cell motility. *Lab Invest*. 2009;89:425–432.
49. Xue X, Lu Z, Tang D, et al. Galectin-1 secreted by activated stellate cells in pancreatic ductal adenocarcinoma stroma promotes proliferation and invasion of pancreatic cancer cells: an in vitro study on the microenvironment of pancreatic ductal adenocarcinoma. *Pancreas*. 2011; 40:832–839.
50. Van den Broeck A, Vankelecom H, Van Eijsden R, et al. Molecular markers associated with outcome and metastasis in human pancreatic cancer. *J Exp Clin Cancer Res*. 2012;31:68.
51. Tian R, Wei LM, Qin RY, et al. Proteome analysis of human pancreatic ductal adenocarcinoma tissue using two-dimensional gel electrophoresis and tandem mass spectrometry for identification of disease-related proteins. *Dig Dis Sci*. 2008;53:65–72.
52. Chen KT, Kim PD, Jones KA, et al. Potential prognostic biomarkers of pancreatic cancer. *Pancreas*. 2014;43:22–27.
53. Powers TW, Neely BA, Shao Y, et al. Maldi imaging mass spectrometry profiling of n-glycans in formalin-fixed paraffin embedded clinical tissue blocks and tissue microarrays. *PLoS One*. 2014;9:e106255.
54. Britton D, Zen Y, Quaglia A, et al. Quantification of pancreatic cancer proteome and phosphorylome: indicates molecular events likely contributing to cancer and activity of drug targets. *PLoS One*. 2014; 9:e90948.
55. Iuga C, Seicean A, Iancu C, et al. Proteomic identification of potential prognostic biomarkers in resectable pancreatic ductal adenocarcinoma. *Proteomics*. 2014;14:945–955.
56. Mirus JE, Zhang Y, Hollingsworth MA, et al. Spatiotemporal proteomic analyses during pancreas cancer progression identifies serine/threonine stress kinase 4 (STK4) as a novel candidate biomarker for early stage disease. *Mol Cell Proteomics*. 2014;13:3484–3496.
57. Faca VM, Song KS, Wang H, et al. A mouse to human search for plasma proteome changes associated with pancreatic tumor development. *PLoS Med*. 2008;5:e123.